Deep-learning-enabled automatic gene abnormality detection via fluorescence in situ hybridization

Cite this as: Lemin SHI, Yuqiang ZHANG, Haoyu QI, Chengyue LU, Menglei HU, Mingye LI, Dianxin SONG, Hao ZHANG, Xin FENG, Ping GONG, Shan JIANG, 2026. Deep-learning-enabled automatic gene abnormality detection via fluorescence in situ hybridization. *Journal of Zhejiang University-SCIENCE A*, 27(3):288-305. https://doi.org/10.1631/jzus.A2500360

Background and Significance

The vast majority of cancers are closely related to gene mutations, which are the root cause of many major diseases. Gene deletion is a common and important genetic abnormality with broad biological and clinical significance, playing a key role in various diseases such as cancer and genetic diseases, especially in the occurrence, development, and drug resistance of tumors.

Fluorescence in situ hybridization (FISH) technology uses fluorescent probes to bind to specific nucleic acid sequences to precisely analyze gene abnormalities at the cellular level. However, this technology has limitations in practical applications, mainly in that it is cumbersome to operate, the results rely on manual interpretation, and it is easily affected by imaging quality and subjective factors, which limits its clinical application.

Method

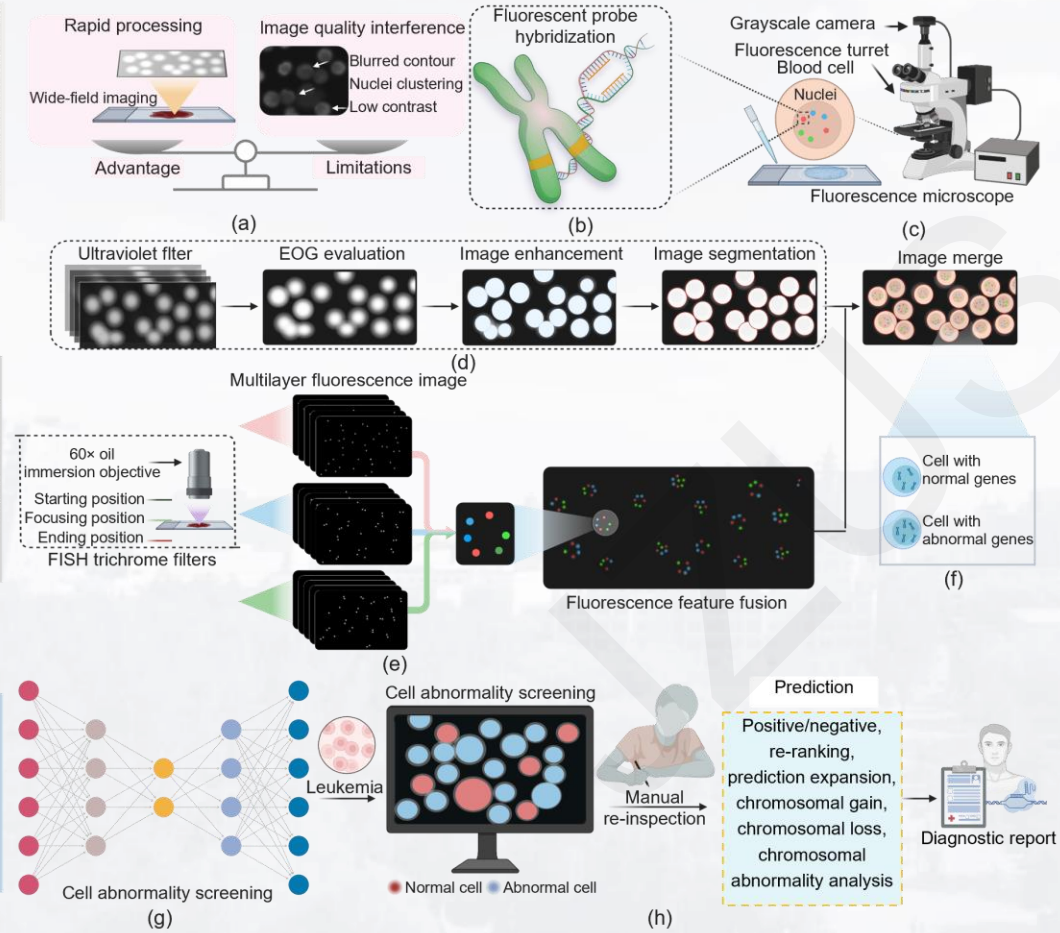


Fig. 1 FAST workflow for cancer diagnosis.
(a) Advantages and limitations of conventional fluorescence microscopy;
(b) FISH probe hybridization targeting specific genetic sequences;
(c) Multilayer image acquisition of hybridized samples using a motorized 2D fluorescence microscope with a grayscale camera and tricolor fluorescence filters;
(d) Image enhancement and segmentation of DAPI-stained nuclei for accurate nuclear contour extraction;
(e) Fusion and analysis of multilayer fluorescence signals from tricolor FISH channels;
(f) Integrated cytogenetic information from all channels for accurate identification and classification of chromosomal abnormalities;
(g) Tailored convolutional neural network (CNN) for automated cell abnormality classification;
(h) User-friendly diagnostic report enabling accurate and efficient cancer diagnosis.
Overall, FAST provides an automated and integrated solution for early cancer detection and personalized prognosis management.

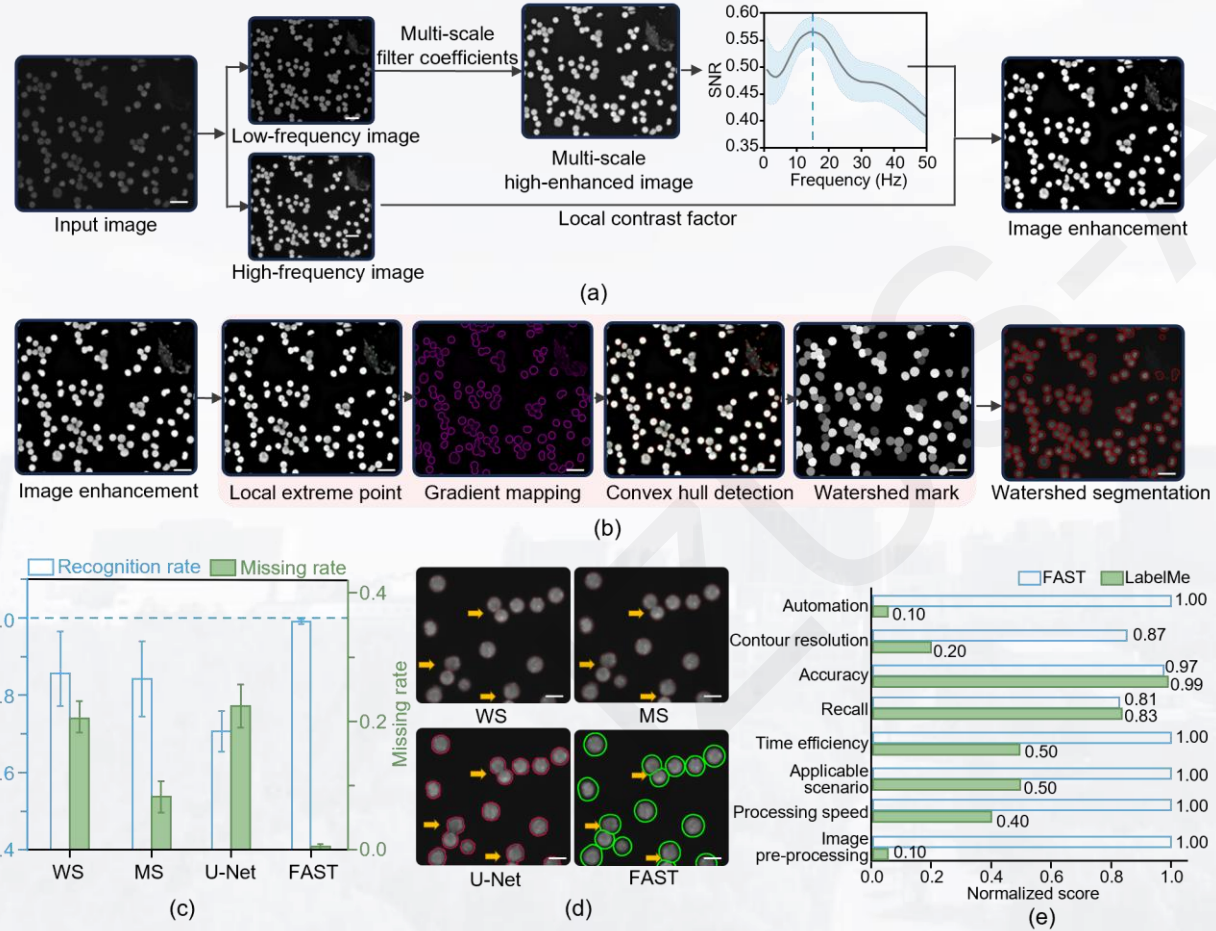


Fig. 2 Image enhancement and nucleus segmentation for accurate nuclear contour identification.

(a) Workflow of image enhancement using a tailored multi-scale DoGs algorithm and image fusion to improve edge sharpness, contrast, and nuclear details;

(b) Accurate nucleus segmentation on representative complex images through local maxima detection, gradient-based feature extraction, convex defect analysis, and iterative seed refinement;

(c) Comparison of nucleus counting accuracy among different segmentation methods;

(d) Qualitative comparison of clustered nucleus segmentation results, with orange arrows highlighting improvements achieved by the proposed method;

(e) Comprehensive performance comparison between FAST and LabelMe in terms of automation, accuracy, recall, time efficiency, and processing speed.

Scale bars: 10 μm in (a) and (b); 5 μm in (d).

MW, MS, and U-Net denote marker-based watershed, morphological segmentation, and a U-Net-based deep learning method, respectively. LabelMe is used as a manual annotation baseline.

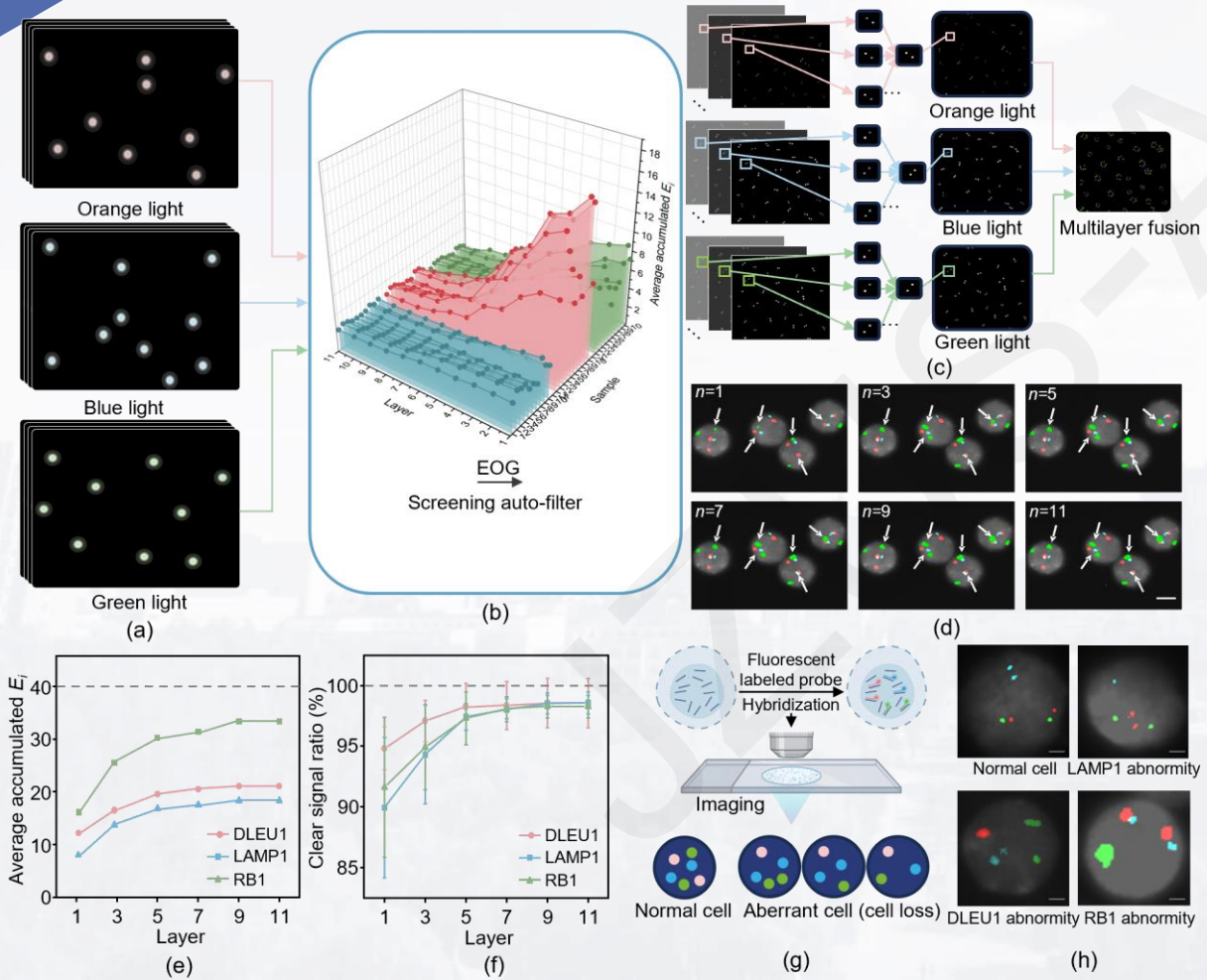


Fig. 3 Multilayer fluorescence feature fusion for chromosomal abnormality screening.
(a) FISH images from different channels showing specific fluorescent signals;
(b) Ranking of fluorescence images based on the energy orientation gradient (EOG) to assess signal clarity;
(c) Automated filtering and multilayer fusion of tricolor fluorescence images;
(d) Comparison of fluorescence signal restoration using n-layer feature fusion (n = 1, 3, 5, 7, 9, and 11), demonstrating progressive signal enhancement with increasing n;
(e, f) Average accumulated EOG values and clear signal ratio across different fusion depths (n = 1, 3, 5, 7, 9, and 11);
(g) Workflow of FISH technology for chromosomal abnormality detection;
(h) Representative FISH patterns showing gene deletions in CLL patients.
Scale bars: 10 μm in (d) and 5 μm in (h).
References to color refer to the online version of this figure.

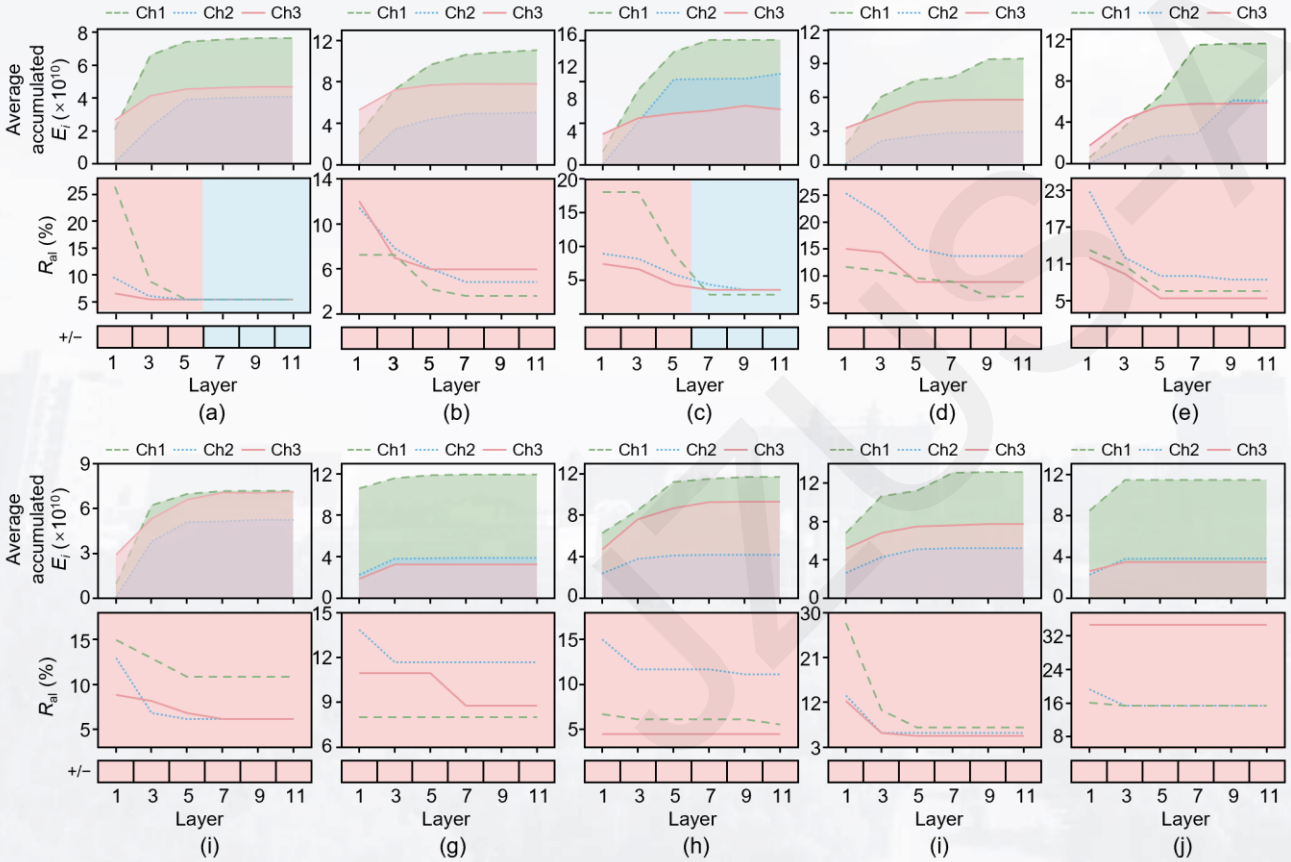


Fig. 4 Evaluation of tricolor fluorescence signal specificity with increasing fusion depth (n). Accumulated Ei and chromosomal abnormality ratios across samples 1–10 (a–j). Shaded regions in the Ral plots and highlighted cells indicate manual classification of chromosomal and corresponding cellular abnormalities, respectively, with red denoting abnormality and blue denoting normality. Symbols “+” and “–” represent positive and negative samples, respectively.
References to color refer to the online version of this figure.

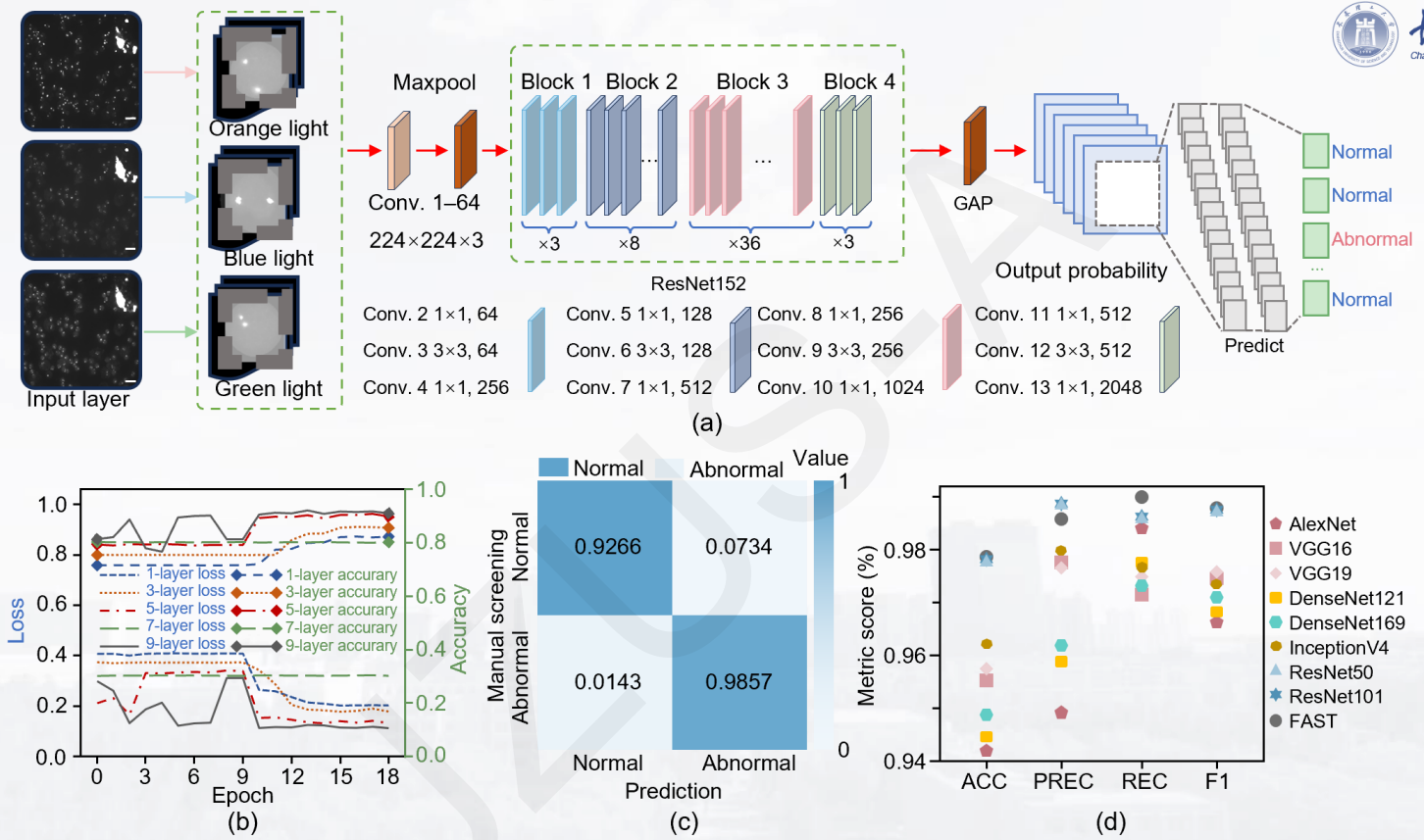


Fig. 5 Deep learning–based cell abnormality detection and cancer diagnosis.
(a) ResNet152-based convolutional neural network (CNN) architecture for automated cell abnormality classification;(b) Learning curves of the ResNet152 model trained with different fusion depths (n = 1, 3, 5, 7, and 9);(c) Confusion matrix comparing ResNet152-based predictions with manual screening across 10 samples; (d) Performance comparison between the proposed method and eight representative deep learning models.Conv. denotes convolution; ACC, PREC, REC, and F1 represent accuracy, precision, recall, and F1-score, respectively.Scale bar: 50 μm in (a). References to color refer to the online version of this figure.

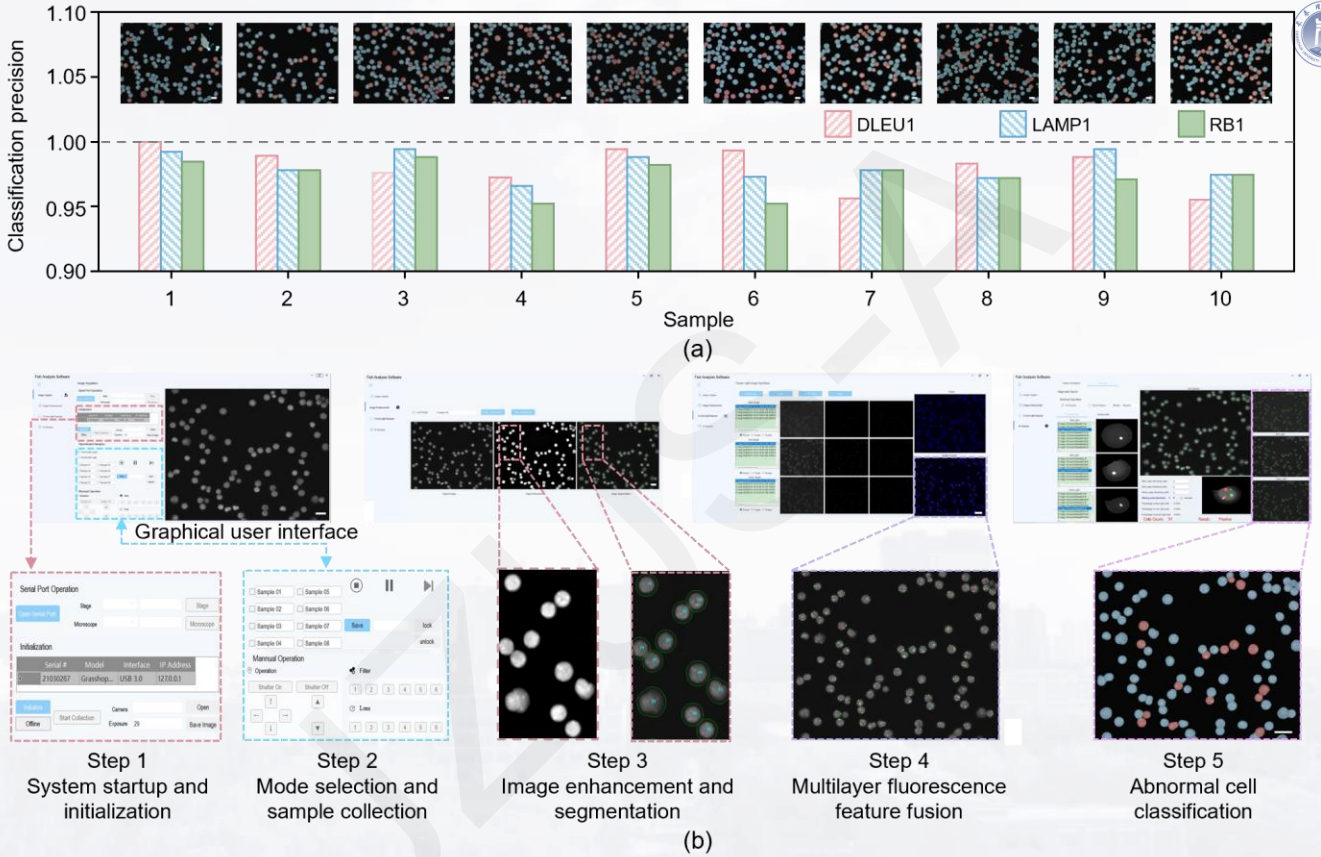


Fig. 6 Abnormality analysis results and system graphical user interface (GUI).

(a) Improved Classification precision of chromosomal abnormalities detected using tricolor fluorescence probes with the ResNet152-based CNN;
(b) Visualization of the GUI and diagnostic report of the integrated FISH imaging and analysis system, designed for non-expert users and supporting early cancer diagnosis and prognostic evaluation. Insets in (a) show representative microscopic images overlaid with color masks, where red and blue indicate abnormal and normal cells, respectively. Scale bars: 50 μm in (a) and (b). References to color refer to the online version of this figure.

Partial experimental results

To further verify the adaptability and generalization ability of multilayer fluorescence feature fusion across various fluorescence channels, this paper evaluates the classification performance of single-channel fluorescence images in three categories: light blue, orange, and green.

